ACS APPLIED MATERIALS & INTERFACES

Research Article

www.acsami.org

Topological Structural Transformations of Nanoparticle Self-Assemblies Mediated by Phase Transfer and Their Application as Organic–Inorganic Hybrid Photodetectors

Yongtao Shen,[†,§] Da Lei,[†,§] Jiahui Tan,[‡,§] Yiyu Feng,[†] Bo Zhang,[†] Yu Li,[†] Huanli Dong,[‡] Wenping Hu,[‡] and Wei Feng*[,†]

[†]School of Materials Science and Engineering, Tianjin Key Laboratory of Composite and Functional Materials, Tianjin University, Tianjin 300072, P. R. China

[‡]Beijing National Laboratory for Molecular Sciences, Institute of Chemistry, Chinese Academy of Sciences (CAS), Beijing 100190, P. R. China

Supporting Information

ABSTRACT: Nanoparticle (NP) self-assemblies have attracted an increasing amount of attention in recent years because of their potential application in the construction of novel nanodevices. The controllable transformation of NP self-assemblies (NPS) between a polar and nonpolar environment is required for many specific applications because of their different properties in different environments. In this article, water-soluble luminescent CdS/CdTe NPS were synthesized using thioglycolic acid as a capping agent. The stiff and straight NPS bundles became loose after phase transfer from an aqueous to an organic phase. Subsequently, the NPS transferred to the aqueous phase. The loose structure transformed into many twisted nanoribbons. Additionally, hybrid photodetectors made using the organic-soluble NPS and P3HT polymers were fabricated, and we found that the NPS/P3HT blend may be perfect for light detection. The organic-soluble NPS are potentially useful for the fabrication of semiconductor nanojunctions.

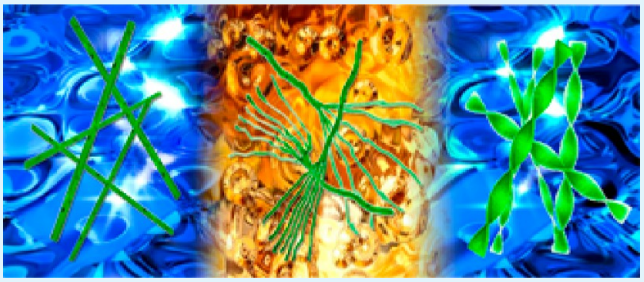

KEYWORDS: *nanoparticle self-assemblies, twisted nanoribbons, phase transfer, structural transformations, photodetectors*

INTRODUCTION

The photonic and electronic properties of nanoparticles (NP) strongly depend on their size, shape, and composition.[1,2] Generally, an individual NP has extremely low electron mobility because no continuous paths exist for efficient charge transport. Therefore, the assembly of NP into self-assemblies by different methods is a hot issue. Electronic coupling between NP neighbors in NP self-assemblies (NPS) counteracts quantum confinement and may result in a reduction of the optical gap, efficient charge mobility for site-to-site hopping, and the formation of continuous paths for carrier transport.[3] These features are favorable for photovoltaic device performance improvements.[4−6] Thus, NPS have attracted an increasing amount of attention owing to their potential for use in the construction of novel nanoarchitectures and nanodevices.[7,8]

Many unusual shapes of NPS, such as nanowires, nanosheets, micelles, vesicles, and binary superlattices, have been reported.[9−21] Among these, Kotov reported a ribbon-shaped NPS that provided a good system to investigate the dependence of electrical and thermal transport or mechanical properties on dimensionality and quantum confinement.[16] Nanoribbons are also expected to play an important role as interconnects and as functional units for the fabrication of electronic, optoelectronic, electrochemical, and electromechanical devices with nanoscale dimensions.[22] However, ribbon-shaped NPS are prepared in an aqueous solution, and it is difficult to produce a compatible blend with nonpolar organic polymers. This type of blend can be obtained by the phase transfer of aqueous-soluble NPS from a polar environment to a nonpolar environment. In this way, NPS enable exciton dissociation at the NPS/polymer interface. Although the phase transfer of individual NP have been reported, the phase transfer of NPS has hardly been studied.

Herein, we report the efficient phase transfer of aqueous-soluble NPS into organic solutions, and these architectures can be applied to the fabrication of photoelectric devices. Aqueous NPS were synthesized using thioglycolic acid (TGA)[6] as a capping agent, and they were transferred to organic solutions. During the phase transfer, an interesting topological transformation of NPS was observed. First, the stiff and straight NPS bundles became loose after phase transfer from the aqueous to the organic phase. This organic-soluble loose NPS formed twisted nanoribbons when using tetramethylammonium dec-

Received: April 21, 2013
Accepted: November 8, 2013
Published: November 8, 2013

Scheme 1. Schematic of the NPS Phase-Transfer Process

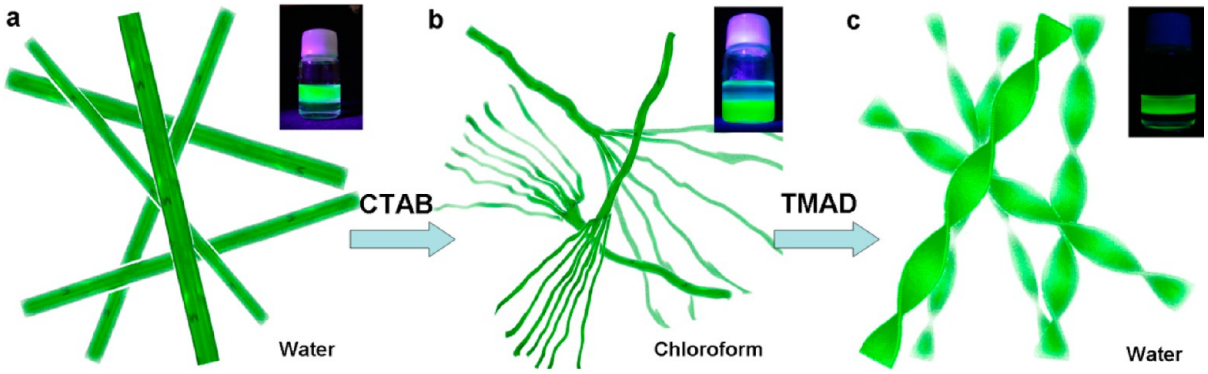

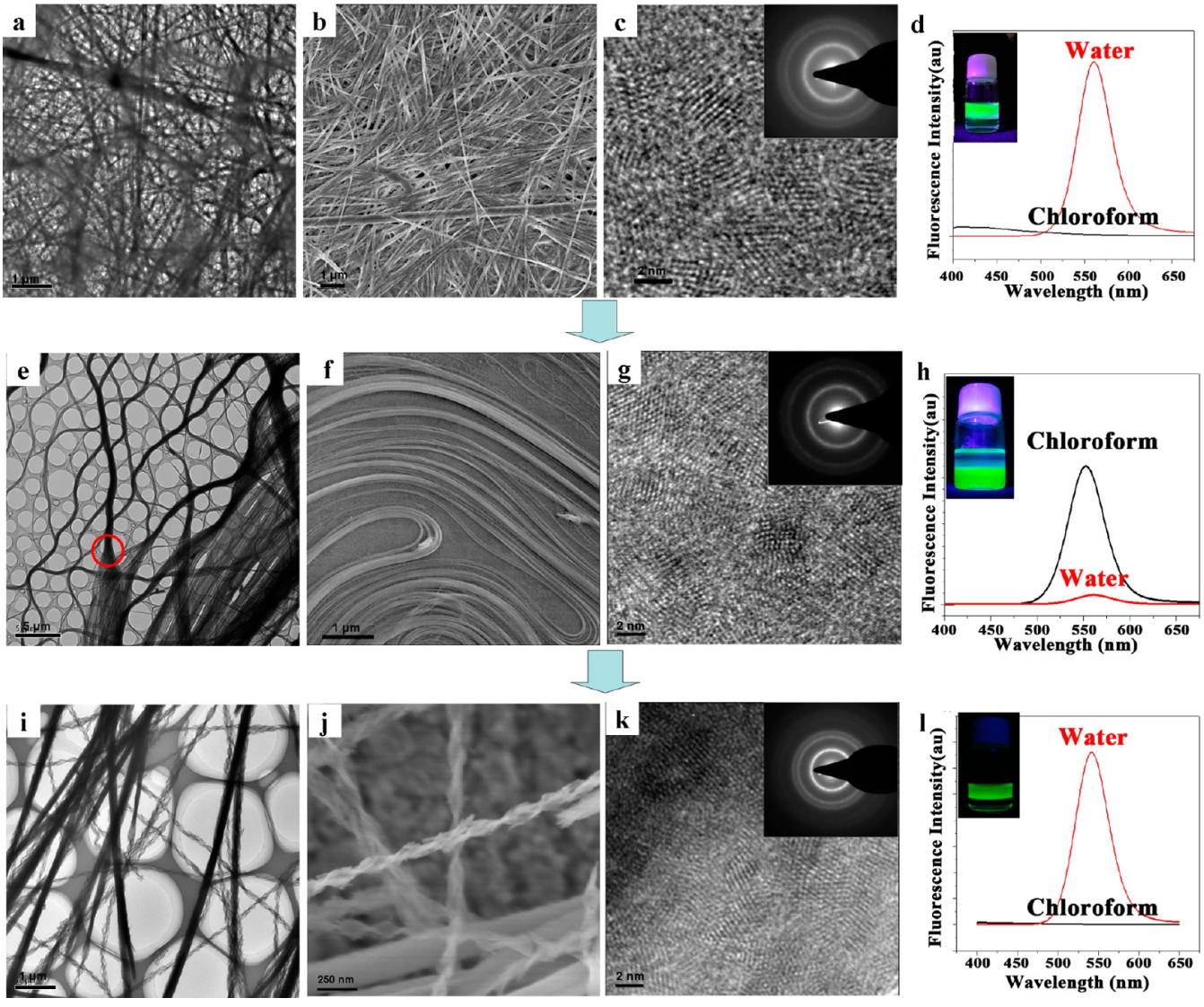

Figure 1. (a, e, i) Typical TEM images and (b, f, j) SEM images of bundles of NPS, loose NPS, and twisted NPS. (c, g, k) HRTEM images for the three kinds of NPS. The insets in images c, g, and k are selected-area electron diffraction (SAED) patterns with diffraction rings. Large SAED images are also shown in Figure S15. The stiff and straight bundles of NPS (as shown in panels a and b) become loose (shown in panels e and f) after phase transfer from the aqueous to the organic phase. Organic-soluble loose NPS form many twisted NPS (shown in panels i and j) after transfer into the aqueous solution as determined using TMAD. (d, h, l) Photoluminescence (PL) spectra of the three kinds of NPS in the chloroform and aqueous phases. The black line is the PL curves of the NPS in chloroform, and the red line is the aqueous phase.

anoate (TMAD) for phase transfer into the aqueous phase (Scheme 1). A hybrid photodetector based on NPS was fabricated. The organic-soluble NPS are useful for the fabrication of advanced semiconductor nanojunctions.

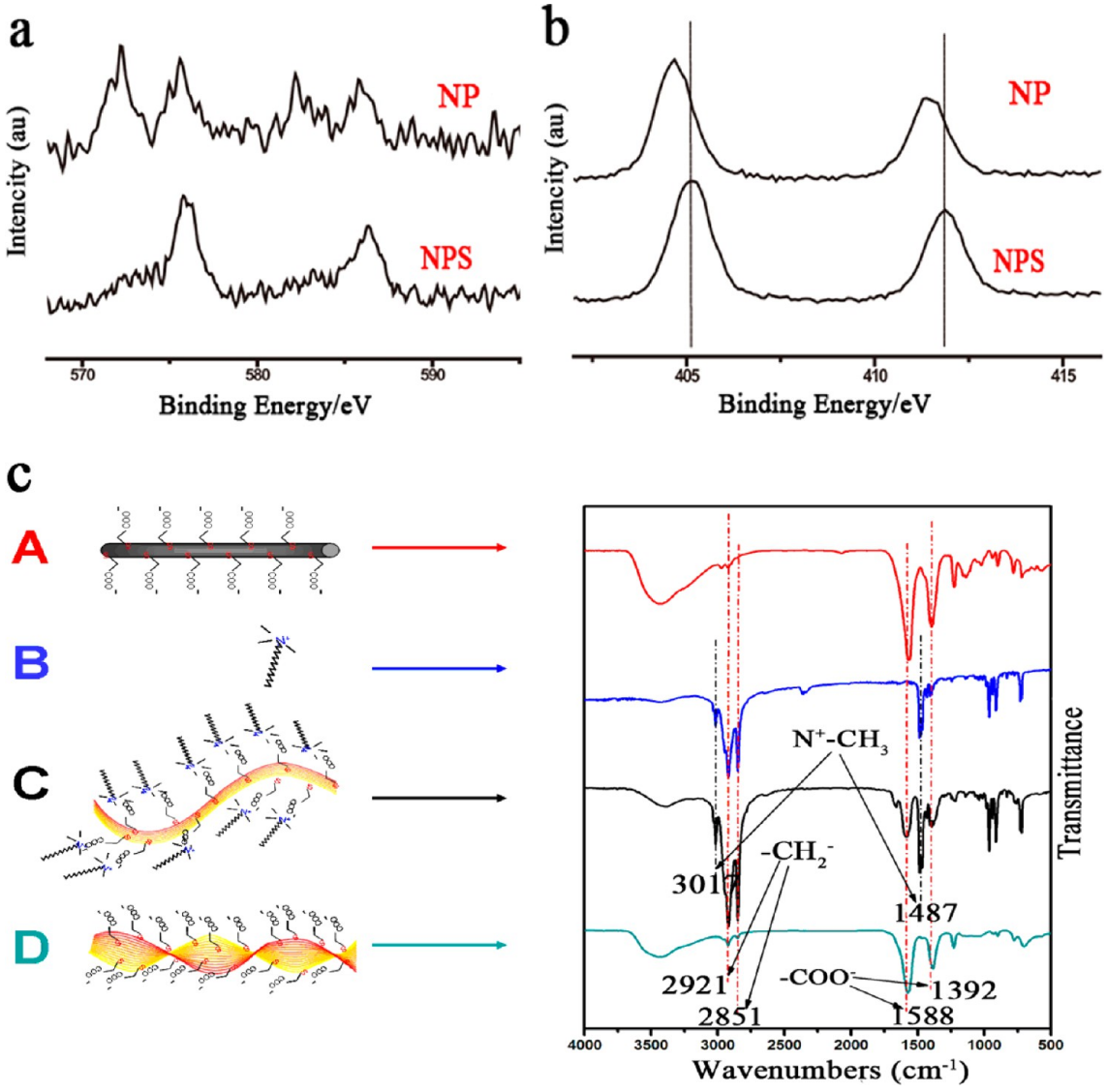

Figure 2. (a, b) XPS results of individual NP and NPS: (a) Te and (b) S. (c) Fourier-transform infrared spectroscopy (FTIR) spectra of (A) original NPS and (B) pure CTAB as well as NPS in (C) chloroform and (D) aqueous phase.

EXPERIMENTAL SECTION

Materials. All chemical reagents were used without further purification. Cadmium perchlorate hydrate ($CdCl_2 \cdot 2.5H_2O$, 99.0%), thioglycolic acid (TGA, $HSCH_2CO_2H$, 98.0%), hexadecyltrimethylammonium bromide (CTAB, 99.0%), decanoic acid (DA, 99.0%), tetramethylammonium hydroxide pentahydrate (TMAH, 98.5%), poly(3-hexylthiophene) (P3HT, 95%), and sodium borohydride ($NaBH_4$, 98.0%) were purchased from Aldrich (Beijing, China). Sodium hydroxide (NaOH, 96.0%) and methanol (H_3COH, 98%) were purchased from Jiangtian Ltd. (Tianjin, China).

Synthesis of NaHTe. Sodium borohydride (80 mg) was transferred to a small flask, and then 3 mL of ultrapure water was added. After 127.5 mg of tellurium powder was added to the flask, the reaction system was cooled using ice. During the reaction, a small outlet connected to the flask was kept open to discharge pressure because of hydrogen generation. After 8 h, the black tellurium powder disappeared, and sodium tetraborate white precipitate appeared at the bottom of the flask. The resulting NaHTe in the clear supernatant was separated and used in the preparation of CdS/CdTe NP.

Synthesis of CdS/CdTe NPS. $CdCl_2$ (0.4 mmol) and TGA (0.6 mmol) were mixed in a 100 mL solution, and the pH of the solution was adjusted to 11.8 by the dropwise addition of a 1.0 M NaOH solution while stirring. The solution was placed in a three-necked flask under argon. While stirring, freshly prepared NaHTe solution (0.3 mmol) was added using a syringe to the $CdCl_2$ solution at room temperature. The mixture was then refluxed at 100 °C under argon with a condenser attached. The reaction was carried out for 8 h. Individually dispersed CdTe NP were obtained and precipitated by the addition of methanol. After centrifugation, the NP were used to fabricate self-assemblies. To reduce the TGA, the precipitates were dissolved in deionized water at a pH of 9 (adjusted by the addition of NaOH). The solution was left to stand, and the NP were self-assembled according to Kotov's methods.[14−16]

Phase Transfer from Aqueous to Organic Solutions. CTAB (3.6 g, 10 mmol) was dissolved in 100 mL of chloroform. Four milliliters of a TGA-stabilized NPS solution was added to 4 mL of the CTAB solution (100 mM). The immiscible mixture was left to stand. After 8 h, the chloroform phase was collected.

Phase Transfer from Organic to Aqueous Solution. Decanoic acid (DA, 1.7 g, 10 mmol) and TMAH (1.8 g, 10 mmol) were dissolved in 100 mL of tetrahydrofuran to form tetramethylammonium decanoate (TMAD, 100 mM). One-half of a milliliter of tetrahydrofuran TMAD solution and 2.5 mL of water were added to 3 mL of chloroform solution containing CTAB-stabilized NPS. The mixture was left to stand. After 12 h, the upper (aqueous) phase was collected.

Fabrication of Photoswitches. P3HT (poly(3-hexylthiophene))[23] (30 mg) was dissolved in 3 mL of chloroform. The NPS chloroform solution (100 μL) and P3HT solution (200 μL) were mixed, and photodetector devices were fabricated by spin coating (2000 rpm) onto precleaned gold electrodes.

RESULTS AND DISCUSSION

Water-Soluble CdS/CdTe NPS. In the aqueous phase, the reduction of the capping agents induces the transformation of NP to NPS because of van der Waals forces and face−face attractions.[14,15,24] Our synthetic mechanism for NPS is based on Kotov's studies.[14−16] Reducing the amount of TGA per NP results in a net decrease in charge repulsion and an increase in the face−face attraction energy, which induces the self-assembly of individual NP. During the first stage, individual NP were synthesized in an aqueous solution at pH 11.8. The repulsion of negative charges on the surface is much stronger than the face−face attraction energy, leading to good stability for NP in aqueous solution. When the NP redissolve into the solution at pH 9, some TGA molecules break away from the individual NP, and the face−face attraction becomes stronger than the repulsion of negative charges on the surface. Such a face−face attraction induces the self-assembly of NP.

To reduce the TGA capping agents, individual NP were precipitated using methanol, the precipitate was then dissolved in deionized water at pH 9 (adjusted by addition of NaOH), and the solution was kept at room temperature under dark conditions for about 1 month. The zeta potential of the solution became substantially more negative during storage, as shown in Figure S1. One-dimensional (1D) NPS was identified in the intermediate self-assembly process, as shown in Figure S2a. These 1D structures self-assembled into hierarchical NPS. The NPS observed are shown in Figure 1a,b. From the SEM image (Figure S2b), the NPS is composed of many nanoribbons, which is shown at the end of the NPS bundles. These NPS thus have "bundle" structures. Energy-dispersive spectroscopy (EDS) was used to determine the composition of the bundle NPS, and the atomic Cd/Te/S ratio was 48.7:1.7:49.6, as shown in Figure S3. The degradation of the thioglyoxylic acid takes place in alkaline solution, and sulfide ions were released into the CdTe NP. The replacement of Te by S in CdTe NP has been reported.[25,26] Thus, the assembly process is associated with a considerable loss of Te and the transition to CdS/CdTe NPS in which the CdS phase is dominant.[33] To confirm this analysis, XPS was used to examine changes on the surface of the TGA-capped NP after the self-assembly process. From the Te 3d spectra shown in Figure 2a, the TGA-capped NP before self-assembly show two characteristic peaks for Te $3d_{5/2}$ and Te $3d_{3/2}$ at 575.2 and 586.3 eV, respectively, and this comes from elemental Te (Te^0). The peaks at 572.0 and 582.8 eV are assigned to Te^{2-} in CdTe. However, the simple substance Te (Te^0) remains after the self-assembly of the NP, indicating that Te^{2-} to Te^0 oxidation occurred. Additionally, the CdTe NP transformed into CdS, as proved by the Cd 3d spectra. The Cd $3d_{5/2}$ at 405.4 eV is assigned to Cd^{2+} in CdS, which is higher than the range reported for CdTe (404.8−405 eV), as shown in Figure 2b.[26]

The bundled NPS are composed of individual NP, as shown by the HRTEM images. Figure 1c shows a HRTEM image of bundled NPS. The SAED pattern of the bundle structures show three characteristic diffraction patterns for the bright circles (d = 0.32, 0.20, and 0.16 nm), and these do not match any stable CdS structures.[27] These results are attributed to S replacing Te in the NPS, which induces many defects in CdS NPS.

Phase Transfer of NPS. The phase transfer of bundled NPS was conducted using hexadecyltrimethylammonium bromide (CTAB). Although the phase transfer of individual NP has been reported, the phase transfer behavior of NPS has hardly been studied. One reason is the pH sensitivity of NPS because the general methods for phase transfer require the modulation of solution pH, which influences the self-assembly of individual NP.[14,15] Another reason is vibration, which is important in the general method for the phase transfer of individual NP.[28−34] However, any vibration might destroy the NPS during phase transfer. Two reasons are thus responsible for the difficulty in NPS phase transfer.

It is well-known that an anionic monolayer covers the surface of the TGA-capped NPS. Cationic groups are presented in CTAB molecules, which can combine with the anionic groups of TGA. Furthermore, CTAB molecules provide sufficient hydrophobicity to facilitate the phase transfer of NPS and to render them soluble in organic solvents. The phase transfer of bundled NPS at different times is shown in Figure S6. The transfer of NPS to chloroform shows two Fourier-transform infrared spectroscopic (FTIR) bands centered at 2850 and 2919 cm^{-1} (Figure 2c), and these are attributed to the symmetric and asymmetric stretching of the methylene groups of CTAB, respectively. The photoluminescence (PL) spectra of CTAB-stabilized NPS in both the organic and aqueous phases are shown in Figure 1h.

Compared with the straight bundle structures, the organic-soluble NPS transforms to a loose structure. Many ribbon structures are dispersed at the end of the formed bundle NPS, as shown in Figure 1e, and this is highlighted by the red circle. Additionally, the width of the undispersed parts of the loose NPS is more than that of the formed bundle NPS. These results indicate that CTAB molecules penetrate the bundle NPS and the bundle NPS separates to form many nanoribbon structures. The SEM image (Figure 1f) also shows the separated loose ribbons.

The loose structures also contain individual NP, as shown by HRTEM. Figure 1g shows the HRTEM image of loose NPS. The SAED pattern of the loose NPS shows a characteristic diffraction pattern for the three bright circles (d = 0.32, 0.20, and 0.16 nm), and these are similar to the bundle NPS obtained in the aqueous phase.

The addition of TMAD molecules results in the transfer of NPS from chloroform to the aqueous phase. The anionic NPS is less hydrophobic per unit charge than the decanoate anion.[39] Therefore, anionic $(NPS)^-$ and cationic $(TMA)^+$ separate in the aqueous phase to form hydrophilic salts. The hydrophobic $(CTA)^+D^-$ compounds separate in chloroform. For this process, tetrahydrofuran, which is miscible with chloroform and a good solvent for TMAD, was used to increase the interfacial contact between the CTAB-stabilized NPS and TMAD. Ligand exchange was completed at the interface between water and chloroform. Therefore, the CTAB-capped NPS transferred to the aqueous phase. Photoluminescence (PL) spectra of the reverse-TGA-stabilized NPS in organic and aqueous phases are shown in Figure 1l. The resulting FTIR spectrum (Figure 2c) is similar to that of the original TGA-stabilized NPS, indicating the dissociation of the $(NPS)^-(CTA)^+$ complex.

The topological structures cannot transform back to their former bundle structures. Many twisted nanoribbons were found after transfer from the organic to the aqueous solution, as shown in Figure 1i,j. The twisted ribbon is composed of many filaments, as shown in Figure S7. Figure 1k shows a HRTEM image of a twisted ribbon. The SAED pattern of the twisted ribbon gave characteristic diffraction patterns for CdS (111) (d = 0.34 nm),

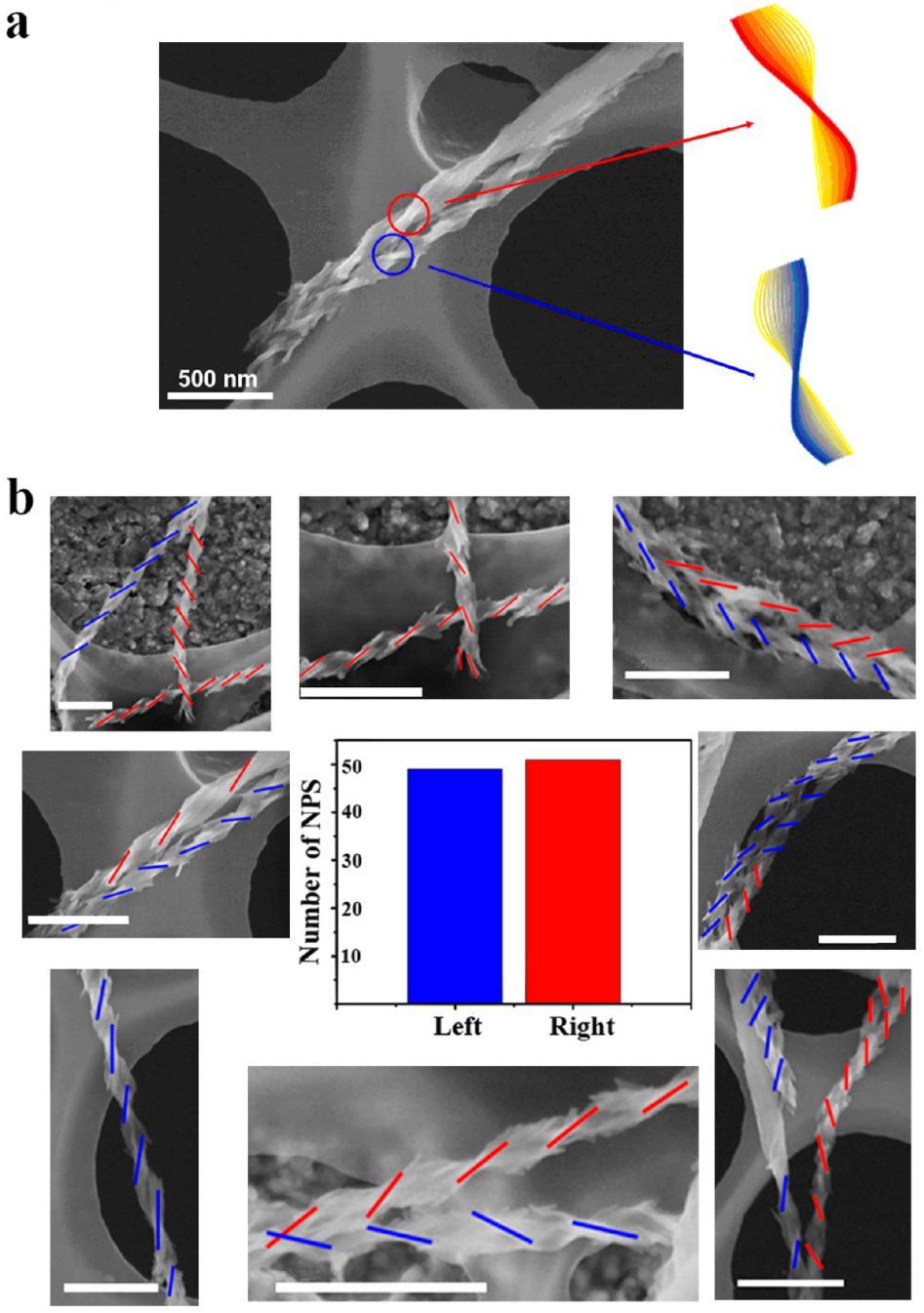

Figure 3. (a) SEM image and a schematic illustration of two kinds of twisted NPS with different chiralities. (b) Distribution of two kinds of NPS with different chiralities (scale bar, 500 nm).

(220) (d = 0.21 nm), and (331) (d = 0.18 nm),[27] which indicates that these twisted ribbons are composed of cubic CdS NP phases and that the crystal lattice of NPS is modulated.

To quantify the transfer process, 3 mL of three kinds of NPS solutions (3 mL each) were precipitated by the addition of 10 mL of methanol followed by centrifugation. The precipitates were collected and rinsed (ultrasound and centrifugation) three times with methanol. This process is useful for the removal of excess CTAB and decanoic acids. The residue was dried and weighed. We obtained 1.2, 6.3, and 0.9 mg of the residues for the three samples. An approximate 5-fold higher precipitate weight was obtained for the organic phase compared with the original aqueous precipitate, which probably indicates that residual CTAB micelles also precipitated. Compared with the bundle NPS aqueous solution and the twisted ribbon aqueous solution, these values correspond to a phase transfer ratio of about 0.75.

Chirality of NPS. The pitch lengths (P) and chirality of the twisted structure were further investigated. Figure 3a shows two kinds of twisted ribbons with different helix chiralities. We found that the amount of both types of twisted chiralities were almost the same, which implies that the twisted ribbons did not have selective chiralities, as shown in Figure 3b. Because of photocorrosion, the stacked nanoparticles were forced to rearrange. Spontaneous symmetry breaking occurred. The stacking pattern may equally follow two directions. The two symmetry breaking directions are equally probable. Eventually, chiral twisted features were observed in the NPS.

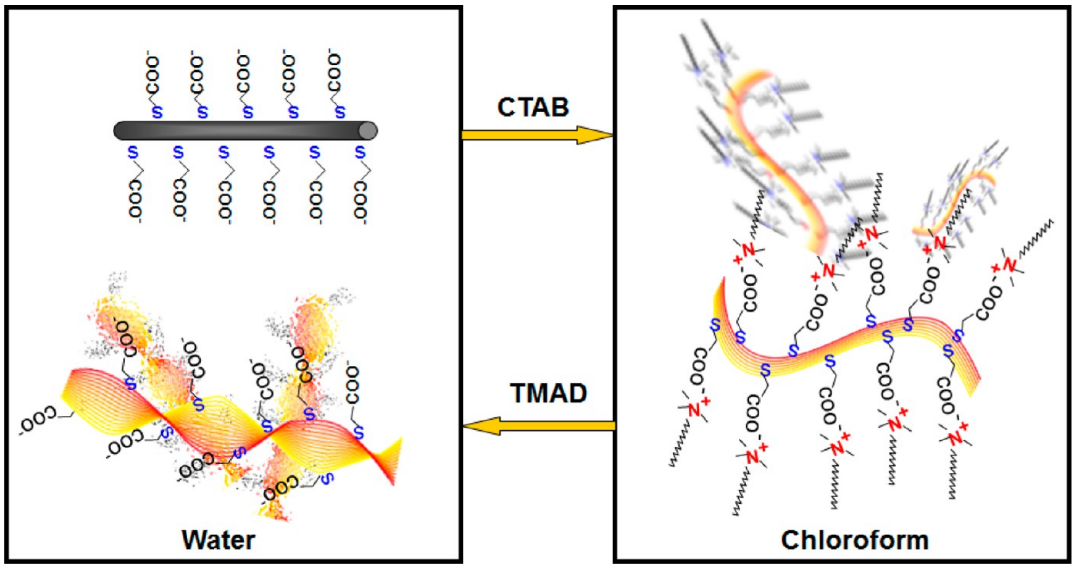

Figure 4. Illustration showing ligand exchange in the NPS phase-transfer process.

The side line of the twisted ribbon can be considered to be a helix line. A helix can be described parametrically by the following equations

$$\begin{cases} x = r \cos t \\ y = r \sin t \\ h = ct \end{cases}$$

where r is the radius, and $c = P/2\pi$. A helix is well-defined if its r and P are specified. From other literature, the pitch-radius ratio (denoted C, $C = P/r$) is used to discuss the optimal shape of closely packed ideal ropes, and the ideal helical conformation with a particular C ($C = 2.5$) can be selected using simulation results.[35,36] In our case, the pitch lengths are different in the twisted ribbons, as shown in Figure S12. However, C was in the range of 2.3−2.7, indicating an approximate ideal helical conformation.

Explanation of Topological Structure Transformation by Phase Transfer. In this article, we show the phase transfer of NPS from an aqueous phase into an organic phase as well as from an organic phase into an aqueous phase. During this process, the topological structures of the NPS changed. Surface changes and the transformation of the NPS structures are shown in Figure 4.

Explanation of the Transformation from a Straight Bundle Structure to a Loose Structure. First, ribbon bundle NPS were prepared. Many negative charges exist on the surface of the bundle NPS because of the carboxyl group of TGA. Therefore, the bundle structures are straight because of the repulsion of negative charges on the surface. When the bundle structure is transferred to an organic phase, the CTAB molecules form salts with the carboxyl of TGA (Figure 4). Thus, the repulsion of negative charges disappears. The bundle structure transforms to a loose structure. Because of the penetration of CTAB molecules, some bundle NPS expand and some bundles even disperse at their ends and form many ribbons.

Explanation of the Transformation from a Loose Structure to Twisted Ribbons. When organic-soluble loose structures are transferred to the aqueous phase, the twisted ribbons can be identified. Typical helical structures originate from specific crystal-lattice distortions, mechanical strains, or chiral building blocks. However, for NPS, Kotov's group reported twisted nanoribbons solely. Their twisted-ribbon structures were associated with the relief of mechanical shear stress in the assembly process, which was caused by the photooxidation of CdS.[16] Herein, we agree with them in that our helix structural transformation can be attributed to a partial photocorrosion. Light irradiation induces photocorrosion, as shown by the XPS results (Figure S9). The XPS results show new peaks in the S_{2p} spectra at 168.0 eV because of photocorrosion by light, as shown in Figure S9. The peak at 168.0 eV corresponds to the S(IV) in sulfite, and this indicates an oxidation of the twist ribbons. In our case, in addition to photocorrosion, light irradiation also induces a rearrangement of the crystal lattice. Therefore, the rearrangement of nanocrystal lattices provides some mechanical shear stress. The rearrangement of nanocrystal lattices can be demonstrated by SAED patterns (Figure 1k). To prove our results, Na_2S was used in the transfer. Na_2S is a sacrificial agent in CdS photocatalysis and can prohibit the photocorrosion of CdS. The results are shown in Figure S13. From the SEM images, the number of separated nanoribbons is more than that without Na_2S. This result shows that Na_2S can prevent the photocorrosion of nanoribbons. Additionally, the nanoribbon is distorted and is not twisted regularly. These results indicate the presence of mechanical shear stress in the nanoribbons without photocorrosion. Because of the absence of photocorrosion, the mechanical shear stress is not released adequately or regularly. Thus, only distorted nanoribbons are obtained.

In conclusion, we postulate that the photocorrosion and rearrangement of the nanocrystal lattices of CdS are combined actions that lead to the structural transformation.

Fabrication of an Organic−Inorganic Hybrid Photodetector. Hybrid organic−inorganic devices can take advantage of both inorganic and organic compound properties while overcoming their own shortcomings.[37] Such devices have been fabricated using several kinds of NP such as $CuInSe_2$ NP,[38] TiO_2 NP,[39] Ge NP,[40] and ZnO NP.[5] However, hybrid organic−inorganic NPS devices have been hardly studied. Herein, a photodetector device comprising an organic-soluble NPS and P3HT hybrid films was fabricated, and it can indirectly verify the miscibility of NPS and P3HT polymers. The UV−vis absorption spectra of NPS, the P3HT film, and the hybrid film were obtained and are shown in Figure S10.

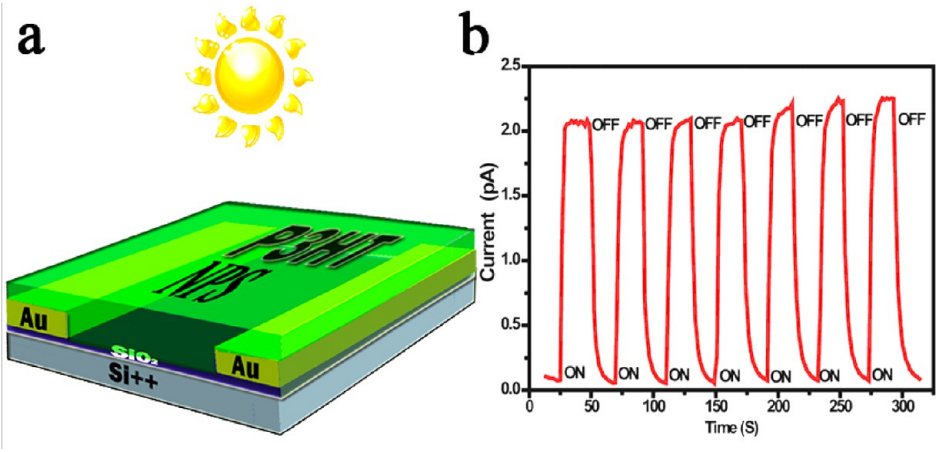

Figure 5. (a) Illustration of the hybrid device. (b) On/off switching of the hybrid device at an incident light intensity of 5.51 mW cm^{-2} and a bias voltage of 1 V.

An illustration of the hybrid device is shown in Figure 5a. The current−voltage (I−V) characteristics of the device were measured with a Keithley 4200 SCS and a Micromanipulator 6150 probe station in a clean and shielded box at room temperature. An iodine−tungsten lamp was used as a white-light source. Figure 5b shows the photocurrents of the device during repetitive switching of light illumination (i.e., on/off switching). The photocurrent increases and decreases in response to the on/off operation and thus it shows photosensitivity. In the dark, the current was only 0.04 pA. At an incident light density of 5.51 mW cm^{-2} and a bias voltage of 1 V, the current increased to 2.3 pA, giving an on/off switching ratio of >50. Further experiments show that the photocurrent is sensitive to the intensity of the incident light, as shown in Figure S14. To understand the photoresponse mechanism of the hybrid material, a blank test was also performed. The change in photocurrent that originates from pure P3HT is relatively low, as shown in Figure S11, which is consistent with other reports.[41] However, the P3HT and NPS hybrid material gives a sharp increase in photocurrent under light illumination, which indirectly verifies the miscibility of the NPS and P3HT polymers. The organic-soluble NPS makes the hybrid material a candidate for light-detection and signal-magnification applications such as a photodetector.

CONCLUSIONS

In this article, water-soluble luminescent CdS/CdTe NPS were synthesized using thioglycolic acid (TGA) as a capping agent. The stiff and straight NPS bundles became loose upon phase transfer from an aqueous to an organic phase. The NPS were then transferred to the aqueous phase again, and the flexible structure transformed into many twisted nanoribbons. Additionally, hybrid photodetectors were fabricated using organic-soluble NPS and P3HT polymers. The organic-soluble NPS can be useful for the fabrication of semiconductor nanojunctions.

ASSOCIATED CONTENT

Supporting Information

Instruments used, energy dispersive spectroscopy, dynamic light scattering data, XPS, SEM and TEM images, and UV/vis spectra. This material is available free of charge via the Internet at http://pubs.acs.org.

AUTHOR INFORMATION

Corresponding Author

*E-mail: weifeng@tju.edu.cn.

Author Contributions

§These authors contributed equally.

Notes

The authors declare no competing financial interest.

ACKNOWLEDGMENTS

This work was supported by the National Basic Research Program of China (grant nos. 2012CB626800 and 2010CB934700), the National Natural Science Foundation of China (grant nos. 51073115, 51003072, 51173127, 51203110, 51103094, and 51273144), the Natural Science Foundation of Tianjin and Youth Science Foundation (12JCQNJC01900), and the Research Fund for the Doctoral Program of Higher Education of China (nos. 20110032110067 and 20110032120021).

REFERENCES

(1) Alivisatos, A. P. *Science* **1996**, *271*, 933−937.
(2) Zhou, Y.; Yang, M.; Sun, K.; Tang, Z.; Kotov, N. A. *J. Am. Chem. Soc.* **2010**, *132*, 6006−6013.
(3) Vanmaekelbergh, D. *Nano Today* **2011**, *6*, 419−437.
(4) Xue, D. J.; Wang, J. J.; Wang, Y. Q.; Xin, S.; Guo, Y. G.; Wan, L. J. *Adv. Mater.* **2011**, *23*, 3704−3707.
(5) Yang, H. Y.; Son, D. I.; Kim, T. W.; Lee, J. M.; Park, W. I. *Org. Electron.* **2010**, *11*, 1313−1317.
(6) Gaponik, N.; Rogach, A. L. *Phys. Chem. Chem. Phys.* **2010**, *12*, 8685−8693.
(7) Huynh, W. U.; Dittmer, J. J.; Alivisatos, A. P. *Science* **2002**, *295*, 2425−2427.
(8) Murray, C. B.; Norris, D. J.; Bawendi, M. G. *J. Am. Chem. Soc.* **1993**, *115*, 8706−8715.
(9) Nozik, A. J.; Beard, M. C.; Luther, J. M.; Law, M.; Ellingson, R. J.; Johnson, J. C. *Chem. Rev.* **2010**, *110*, 6873−6890.
(10) Guo, C. X.; Yang, H. B.; Sheng, Z. M.; Lu, Z. S.; Song, Q. L.; Li, C. M. *Angew. Chem., Int. Ed.* **2010**, *49*, 3014−3017.
(11) Nikolic, M. S.; Olsson, C.; Salcher, A.; Kornowski, A.; Rank, A.; Schubert, R.; Frömsdorf, A.; Weller, H.; Förster, S. *Angew. Chem., Int. Ed.* **2009**, *48*, 2752−2754.
(12) Schliehe, C.; Juarez, B. H.; Pelletier, M.; Jander, S.; Greshnykh, D.; Nagel, M.; Meyer, A.; Föerster, S.; Kornowski, A.; Klinke, C.; Weller, H. *Science* **2010**, *329*, 550−553.

(13) Shevchenko, E. V.; Ringler, M.; Schwemer, A.; Talapin, D. V.; Klar, T. A.; Rogach, A. L.; Feldmann, J.; Alivisatos, A. P. *J. Am. Chem. Soc.* **2008**, *130*, 3274−3275.
(14) Tang, Z. Y.; Zhang, Z.; Wang, Y.; Glotzer, S. C.; Kotov, N. A. *Science* **2006**, *314*, 274−279.
(15) Tang, Z. Y.; Kotov, N. A.; Giersig, M. *Science* **2002**, *297*, 237−240.
(16) Srivastava, S.; Santos, A.; Critchley, K.; Kim, K. S.; Podsiadlo, P.; Sun, K.; Lee, J.; Xu, C. L.; Lilly, G. D.; Glotzer, S. C.; Kotov, N. A. *Science* **2010**, *327*, 1355−1359.
(17) Zhang, H.; Edwards, E. W.; Wang, D.; Möhwald, H. *Phys. Chem. Chem. Phys.* **2006**, *8*, 3288−3299.
(18) Ding, J.; Wang, X.; Zhuo, L. H.; Tang, B. *J. Mater. Chem.* **2009**, *19*, 3027−3032.
(19) Liu, Y. H.; Wang, F. D.; Wang, Y. Y.; Gibbons, P. C.; Buhro, W. E. *J. Am. Chem. Soc.* **2011**, *133*, 17005−17013.
(20) Zhang, H.; Wang, D.; Möhwald, H. *Angew. Chem., Int. Ed.* **2006**, *45*, 748−751.
(21) Zhang, H.; Wang, D.; Möhwald, H. *J. Am. Chem. Soc.* **2006**, *128*, 10171−10180.
(22) Xia, Y.; Yang, P.; Sun, Y.; Wu, Y.; Mayers, B.; Gates, B.; Yin, Y.; Kim, F.; Yan, H. *Adv. Mater.* **2003**, *5*, 353−389.
(23) Holdcroft, S. *Macromolecules* **1991**, *24*, 4834−4838.
(24) Zhang, Z.; Tang, Z. Y.; Kotov, N. A.; Glotzer, S. C. *Nano Lett.* **2007**, *7*, 1670−1675.
(25) Bao, H. B.; Gong, Y. J.; Li, Z.; Gao, M. Y. *Chem. Mater.* **2004**, *16*, 3853−3859.
(26) Chen, Y. J.; Yan, X. P. *Small* **2009**, *5*, 2012−2018.
(27) Sharma, R. C.; Chang, Y. A. *J. Phase Equilib.* **1996**, *17*, 425−431.
(28) Jiang, H. B.; Jia, J. G. *J. Mater. Chem.* **2008**, *18*, 344−349.
(29) Qiu, P. H.; Jensen, C.; Charity, N.; Towner, R.; Mao, C. B. *J. Am. Chem. Soc.* **2010**, *132*, 17724−17732.
(30) Dong, A. G.; Ye, X. C.; Chen, J.; Kang, Y. K.; Gordon, T.; Kikkawa, J. M.; Christopher, B. M. *J. Am. Chem. Soc.* **2011**, *133*, 998−1006.
(31) Bai, S.; Wu, C. Z.; Gawlitza, K.; Klitzing, R. V.; Marion, B.; Schumacher, A.; Wang, D. Y. *Langmuir* **2010**, *26*, 12980−12987.
(32) Gaponik, N.; Talapin, D. V.; Rogach, A. L.; Eychmüller, A.; Weller, H. *Nano Lett.* **2002**, *2*, 803−806.
(33) Qin, B.; Zhao, Z. Z.; Song, R.; Shanbhag, S.; Tang, Z. Y. *Angew. Chem., Int. Ed.* **2008**, *47*, 9875−9878.
(34) Wei, Y. F.; Yang, J.; Ying, J. Y. *Chem. Commun.* **2010**, *46*, 3179−3181.
(35) Snir, Y.; Kamien, R. D. *Science* **2005**, *307*, 1067−1067.
(36) Maritan, A.; Micheletti, C.; Trovato, A.; Banavar, J. R. *Nature* **2000**, *406*, 287−290.
(37) Bousquet, A.; Boyer, C.; Davis, T. P.; Stenzel, M. H. *Polym. Chem.* **2010**, *1*, 1186−1195.
(38) Wang, J. J.; Wang, Y. Q.; Cao, F. F.; Guo, Y. G.; Wan, L. J. *J. Am. Chem. Soc.* **2010**, *132*, 12218−12221.
(39) Han, Y.; Wu, G.; Wang, M.; Chen, H. *Polymer* **2010**, *51*, 3736−3743.
(40) Xue, D. J.; Wang, J. J.; Wang, Y. Q.; Xin, S.; Guo, Y. G.; Wan, L. J. *Adv. Mater.* **2011**, *23*, 3704−3707.
(41) Barus, S.; Zanetti, M.; Lazzari, M.; Costa, L. *Polymer* **2009**, *50*, 2595−2600.